Biomass Conversion and Biorefinery (2023) 13:11983–11996
https://doi.org/10.1007/s13399-022-02305-7

ORIGINAL ARTICLE

Effective degradation of amoxicillin using peroxymonosulfate activated with MWCNTs-CuNiFe2O4 as a new catalyst: optimization, degradation pathway, and toxicity assessment

Abdolrasoul Rahmani[1] · Nezamaddin Mengelizadeh[1] · Mohammad Darvishmotevalli[2] · Mehdi Salari[3] · Maryam Moradnia[4] · Mohammad Noorisepehr[2] · Habibeh Nasab[5] · Mina Rostami[4] · Bahador Nemati[6] · Majid Hashemi[5] · Sara Ashrafi[7]

Received: 22 July 2021 / Revised: 31 December 2021 / Accepted: 3 January 2022 / Published online: 14 January 2022

Abstract

In this study, copper-nickel ferrite ($CuNiFe_2O_4$) nanoparticles were fabricated on multi-walled carbon nanotubes (MWCNTs) by co-precipitation method and used to activate peroxymonosulfate (PMS) for amoxicillin (AMX) degradation in aqueous solution. Scanning electron microscope (SEM), transmission electron microscopy (TEM), X-ray powder diffraction (XRD), and Fourier transform infrared spectroscopy (FTIR) analyses were performed for the surface morphology and physico-chemical properties of the catalyst. High catalytic activity for AMX degradation by MWCNTs-$CuNiFe_2O_4$/PMS system (100%) was achieved at a reaction time of 120 min compared to other heterogeneous systems such as Fe_3O_4/PMS (67.85%), $CuFe_2O_4$/PMS (83.2%), and $NiFe_2O_4$/PMS (76.56%). The AMX degradation efficiency increased with increasing dosage of PMS and catalyst, while it decreased with the presence of high AMX concentration and different anions. For four consecutive reaction cycles, the degradation efficiency of AMX did not decrease significantly, indicating the good reusability of MWCNTs-$CuNiFe_2O_4$ in long-term treatment of AMX solution. Quenching tests showed that sulfate ($SO_4^{\bullet-}$) and hydroxyl ($HO^{\bullet}$) radicals are the main reactive species in AMX degradation. The high BOD_5/COD ratio emphasizes that the present catalytic process can oxidize AMX to the compounds with low molecular weight. The presence of NH_4^+, NO_3^-, and SO_4^{2-} ions in the treated effluent indicates that AMX is well mineralized. Toxicity tests performed by culture of *Escherichia coli* and *Staphylococcus aureus* explained that the MWCNTs-$CuNiFe_2O_4$/PMS system could reduce the toxicity of the major contaminant and its byproducts. The AMX degradation pathway was proposed through the identification of intermediates by gas chromatography-mass spectrometry (GC–MS).

Keywords Peroxymonosulfate · MWCNTs-$CuNiFe_2O_4$ · Degradation pathways · Toxicity · Stability

✉ Mohammad Darvishmotevalli
Mohamad.darvish68@gmail.com

✉ Mehdi Salari
msalari_22@yahoo.com

[1] Research Center of Health, Safety and Environment, School of Health, Larestan University of Medical Sciences, Lar, Iran

[2] Research Center for Health, Safety and Environment (RCHSE), Alborz University of Medical Sciences, Karaj, Iran

[3] Department of Environmental Health Engineering, School of Health, Hamadan University of Medical Sciences, Hamadan, Iran

[4] Department of Environmental Health Engineering, School of Public Health, Isfahan University of Medical Sciences, Isfahan, Iran

[5] Environmental Health Engineering Research Center, Kerman University of Medical Sciences, Kerman, Iran

[6] Department of Environmental Health Engineering, School of Health, Kashan University of Medical Sciences, Kashan, Iran

[7] Department of Environmental Health Engineering, School of Public Health, Mazandaran University of Medical Sciences, Sari, Iran

1 Introduction

Concerns about contamination of water resources with emerging compounds, especially pharmaceuticals and personal care products (PPCPs), have increased due to high consumption, low body uptake, structural complexity, and low biodegradability [1–4]. These substances, as stable and bioactive micro-pollutants, have the potential to be dangerous to ecosystems and human health through biological accumulation [5–8]. Beta-lactam antibiotics such as amoxicillin (AMX) with a bacterial cell wall synthesis mechanism are one of the most common PPCPs for the treat of human and animal infections. Due to the amphoteric properties of AMX, a small amount of it is metabolized in the human body and 80–90% is excreted unchanged [6, 9]. Various studies have reported AMX concentrations in the range of ng/L to µg/L in surface water, pharmaceutical industry effluent, and municipal wastewater treatment plants [10]. The presence of these compounds in aqueous media directly and indirectly leads to increasing the antibiotic resistance genes in bacteria and cancer in humans [9]. Unfortunately, biological treatment technology has been inadequate to remove antibiotics due to its toxicity and complex structure. Recently, physicochemical technologies such as adsorption, membrane filtration, and ozonation have been developed to effectively remove persistent contaminants prior to biological processes. However, these techniques have disadvantages such as deposal of adsorbed pollutants, clogging of membranes, and high cost of ozone production [11–13].

Advanced oxidation processes (AOPs) have been considered as an efficient method for removing antibiotics from aqueous solutions due to their simplicity of operation and cost-effectiveness [14]. This process involves reactive oxygen species (ROSs) produced through the oxidation of water, hydroxyl ions, and the activation of oxidants in the mineralization of toxic and refractory compounds [15]. Recently, peroxymonosulfate (PMS) based AOPs has found special attention for wastewater engineers due to the rapid production of $SO_4^{\bullet-}$ through the decomposition of the asymmetric structure of HO-O-SO_3. Sulfate radicals have a higher oxidation potential than $HO^{\bullet}$ (3.1– 5 V vs 1.8–2.7 V of $HO^{\bullet}$), a longer half-life (40 µs vs 20 ns of $HO^{\bullet}$), and greater selectivity in catalytic degradation reactions [16, 17]. Typically, $SO_4^{\bullet-}$ can be produced through PMS activation by UV, heat, ultrasound, and transition metals, of which cobalt is the most widely used due to its abundance, rapid activation, and low energy consumption [18]. However, the cobalt homogenous catalyst is improper for practical applications due to its toxicity and the change of metal species at different pH. For overcoming these disadvantages, ferrite spinel nanoparticles (MFe_2O_4) were proposed in catalysis applications due to their excellent thermal stability, high catalytic activity, and good magnetic properties [19]. Kazemi et al. [20] reported that the catalytic activity of MFe_2O_4 is improved through electron transfer between tetrahedral and octahedral sites. Nickel ferrites ($NiFe_2O_4$) as a common member of spinel ferrites showed good stability in the production of reactive species from ozone decomposition and PMS. In addition, its unique properties such as reduction current loss, high electrical stability, corrosion resistance, and super-paramagnetic have led to applications in the manufacture of drugs, sensors, and catalysts [21, 22]. Kesavan et al. [21] synthesized $NiFe_2O_4$ and used it as an efficient electrocatalyst to electrochemically identify bisphenol A from aqueous solutions. Wang et al. [22] synthesized $NiFe_2O_4$ used in heterogeneous catalysis system to activate peroxymonosulfate for the degradation of organic pollutants by powerful radicals and found the degradation efficiency of 82.5% benzoic acid in reaction time of 60 min with minimal nickel ion leaching. Despite these studies and the high efficiency of ferrites, researchers have recently become interested in mixed ferrites such as $CuNiFe_2O_4$ to ensure multifunctional, excellent stable catalysts, and their high coactivity [23, 24].

Nickel-copper ferrite belongs to mixed ternary-transition-metal ferrites, are described by the formula ($A_xB_{1-x}Fe_2O_4$), where A and B are divalent metal ions (e.g., Cu, Mn, Ni, Zn,). The distribution of these cations in mixed ferrites affects the surface properties, catalytic activity, semiconducting properties, and chemical stability. In addition, the presence of some cations such as Cu in the structure of $A_xB_{1-x}Fe_2O_4$ significantly reduces the toxicity of ferrites. Mixed ferrites are now widely used as adsorbents, catalysts, and supercapacitor electrodes [25, 26]. However, these types of nanoparticles tend to accumulate in practical applications due to their high energy level. To solve this problem, the researchers proposed combining ferrites with carbonic materials [24, 27, 28]. Among carbon materials and sheets, carbon nanotubes (CNTs) have shown unique properties such as excellent mechanical stability, good chemical stability, and suitable electrical conductivity. Carbon nanotubes as a cylinder fabricated of rolled up grapheme sheet contain a large number of functional groups (such as carboxyl and hydroxyl groups) that provide immobilization of large amounts of metal cations with suitable dispersion [29–32]. In CNTs/MFe_2O_4 systems, CNTs activate oxidants such as persulfate and PMS to produce active radicals and then facilitate the transfer of electrons between metal ions with high electrical conductivity to regenerate the catalytic center and oxidation of organic pollutants. In addition, in the high surface area and large pore structure, CNTs have recently been developed as a candidate for pollutant adsorption and nanoparticle support [33–35]. Singhal et al. [36] investigated

the photocatalytic degradation of methylene blue using the MWCNTs/$ZnFe_2O_4$ composite and found that the efficiency of the MWCNTs/ZnF_2O_4 photocatalyst was much higher than that of $ZnFe_2O_4$ due to the effect of CNTs on limiting recombination of photogeneration charge. Synthesis of MWCNTs/TiO_2-Au for antibacterial activity was performed by Karthika and Arumugam [37] and the results showed that the presence of nanotubes in the composite leads to better penetration of nanoparticles for destroying the cell wall. Despite these studies, PMS activation performance by MWCNTs-$CuNiFe_2O_4$ for AMX degradation has not been reported. Moreover, little study has been performed on the identification of anions produced through AMX degradation and toxicity of solution treated by MWCNTs-$CuNiFe_2O_4$/PMS system.

In this study, MWCNTs-$CuNiFe_2O_4$ nanoparticles were synthesized by co-precipitation and used as new activator of PMS for AMX degradation. The influence of important parameters such as initial pH, catalyst dosage, PMS dosage, initial AMX concentration, and anions was evaluated. The mineralization study was performed based on total organic carbon (TOC), biochemical oxygen demand for five day (BOD_5), and chemical oxygen demand (COD) measurements, and stability and recyclability were tested in 5 consecutive reaction cycles. Trapping tests were performed to determine the reactive species in the degradation of AMX and the toxicity of the treated solution was determined using *Escherichia coli (E. coli)* and *Staphylococcus aureus (S. aureus)*. AMX degradation products were analyzed by GC–MS, and the degradation mechanism was proposed based on the results.

2 Material and methods

2.1 Materials

Amoxicillin (AMX, purity ≥ 97%) and peroxymonosulfate (commercial name oxone, $KHSO_5.0.5KHSO_4.0.5K_2SO_4$) were purchased from Sigma Aldrich, USA. Ferric chloride ($FeCl_3.6H_2O$, purity 97%), cupric nitrate ($Cu(NO_3)_2.3H_2O$, purity 99%), nickel nitrate ($Ni(NO_3)_2.6H_2O$, purity 99.99%), sodium hydroxide (NaOH, purity 98%), ethanol (EtOH), tert-butyl alcohol (TBA), and benzoquinone (BQ, > 98%) were provided by Merck, Germany. Acetonitrile and acetic acid used in HPLC analysis were purchased from Merck, Germany. Multi-walled carbon nanotubes (MWCNTs, purity > 95%, inner diameter: 5–10 nm, and length: 10–30 µm) were purchased from US nanomaterial company (LA, USA). All materials used in the present study were analytical grade, and the solutions were prepared with deionized water, except the experiments related to the study of the ionic effect, where chloride ion (Cl-) was added to deionized water.

2.2 Synthesis and characterization of MWCNTs-$CuNiFe_2O_4$

MWCNTs-$CuNiFe_2O_4$ nanocatalyst was prepared by co-precipitation as shown in Fig. 1. Briefly, 2 g MWCNTs was dispersed in 100 mL of distilled water for 30 min, and then 1 g $FeCl_3.6H_2O$, 0.5 g $Cu(NO_3)_2.3H_2O$, and 0.25 g $Ni(NO_3)_2.6H_2O$ were added to the mixing solution. The pH was adjusted above 11 by 2 M NaOH and the solution temperature was raised to 80 °C. The mixture was kept on a stirrer for 2 h and finally the solid product was washed on the filter with distilled water until reaching neutral pH and dried at 60 °C in an oven for 24 h.

Structural properties and particle size of MWCNTs-$CuNiFe_2O_4$ were determined by scanning electron

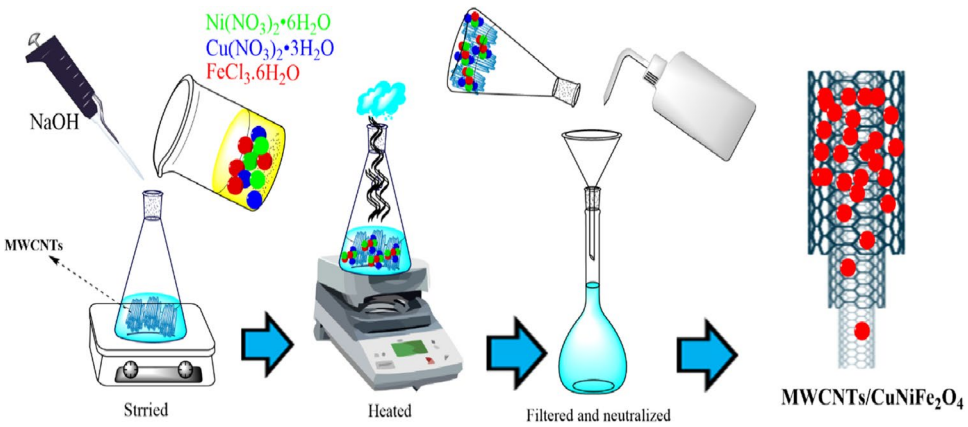

Fig. 1 Schematic illustration of the formation of MWCNTs-$CuNiFe_2O_4$ nanocomposite

microscopy (SEM, MIRA III model, TESCAN Co.) and transmission electron microscope (TEM, CM120 model, Netherlands). Sample element analysis was evaluated by energy dispersive X-ray (EDX) mapping (MIRA III model, TESCAN Co.). The crystalline structure of the catalyst was determined by X-ray diffractometer (XRD, PW1730 model, Philips Co.) with Cu Kα radiation in the scanning range of 10 to 80°. FTIR spectra samples were recorded in the range of 400 to 4000 cm^{-1} using an AVATAR spectrometer (Thermo Co., USA).

2.3 Experimental procedures

AMX degradation tests were performed on a 250-mL Erlenmeyer. Weighed amounts of MWCNTs-$CuNiFe_2O_4$ and PMS were added in 100 mL of solution containing 50 mg/L AMX, and the mixture was stirred at 200 rpm by magnetic stirrer at room temperature (25 ± 2 °C). Effect of various parameters such as initial pH (3–11), catalyst dosage (100–1000 mg/L), PMS dosage (0.5–7 mM), and initial AMX concentration (2–75 mg/L) at constant solution temperature of 15 °C was investigated on catalytic degradation of AMX. The pH of the reaction solution was adjusted by 0.1 M H_2SO_4 and 0.1 M NaOH. At various intervals, 2 mL sample was taken from the reactor and filtered by a 0.2-µm filter to separate solids. All experiments were repeated three times, and only the mean value was reported.

Stability tests were performed to evaluate the reusability of MWCNTs-$CuNiFe_2O_4$ in the PMS activation system. The catalysts were separated after each reaction cycle by a filter, washed with distilled water, and dried in an oven at 60 °C. Trapping test was performed to determine ROSs produced by the MWCNTs-$CuNiFe_2O_4$/PMS system. A total of 10 mM TBA, EtOH, and BQ were used as scavengers of ROSs and poured separately into the reaction solution. The process was run at optimal operational conditions, and the removal efficiency of AMX was determined. By comparing the removal efficiency of AMX in the presence and absence of scavenger radicals, we suggested the main probable radicals involved in the oxidation process.

2.4 Analytical methods

The remaining AMX in the reactor was measured by high-performance liquid chromatography (HPLC) coupled with a C18 column (4.6 nm, 250 nm, and 5 µm). The mobile phase was a mixture of acetonitrile and 0.1% acetic acid at 20:80 (V/V). Limit of detection (LOD) and limit of quantification (LOQ) of HPLC instrument were determined to be 0.1 and 0.3 mg/L, respectively. The elution of AMX profile was monitored with a UV detector with a wavelength of 230 nm. Total organic carbon was measured by a TOC analyzer (Teledyne Tekmar TOC Torch). Sulfate (SO_4^{2-}), nitrate (NO_3^-), and ammonium (NH_4^+) ions were determined according to standard methods for the examination of water and wastewater.

AMX degradation products from the MWCNTs-$CuNiFe_2O_4$/PMS system were detected by GC–MS coupled with dispersive liquid–liquid microextraction (DLLME). Prior to analyses, 5 mL of the sample was pretreated with dichloromethane, and 2 µL of the precipitated solution was injected into a GC equipped with an Agilent 5975C MSD mass spectrometer and electron ionization (EI) mode. The DB-5 column of GC was operated for 4 min at a temperature of 120 °C and then increased to 300 °C at a temperature of 20 °C/min and, finally, was maintained at 300 °C for 5 min. Byproduct analysis was performed in full scan mode at 50–1000 m/z and interpreted by mass spectral libraries (NIST 20 and Wiley Libraries). Ion source, detector, and injector temperatures were set at 230, 300, and 220 °C, respectively. Inductively coupled plasma mass spectrometry (ICP-MS) analysis was applied to study the values of Fe, Ni, and Cu elements leached to the reaction solution, using ICP–OES (Optima-8300) instrument. COD content was quantified by using high-range COD ampoules (HACH Chemical) by the UV–visible spectrophotometer. The BOD_5 value of the real wastewater was measured by the manometric method using a respirometer (BSB-Controller model 620 T, WTW).

2.5 Toxicity test

E. coli and *S. aureus* were used to evaluate the toxicity due to the presence of high amounts in aqueous media. Lactose broth culture medium was prepared, and 16 tube tests containing broth for each bacterium were sterilized in an autoclave. Simultaneously, *E. coli* and *S. aureus* were incubated in EMB agar and nutrient agar at 37 °C for 24 h, respectively. For each microorganism, 4 tubes were used as a control test and 4 tubes as a toxicity test in the optimal condition (10 mL of culture medium + 1 mL reactor outlet + one loop of microbe). After incubation at 37 °C, absorbance of test tubes was performed by UV–vis spectrophotometry at 600 nm.

3 Results and discussion

3.1 Characterizations of MWCNTs-$CuNiFe_2O_4$

The surface morphology of MWCNTs, $CuNiFe_2O_4$, and MWCNTs-$CuNiFe_2O_4$ was tested by SEM analysis, and the results were shown in Fig. 2. As can be seen, the mixed ferrite nanoparticles were spherical (Fig. 2b) and were well formed on the wall of MWCNTs. The swelling of the MWCNTs in Fig. 2c and d emphasizes that $CuNiFe_2O_4$ is

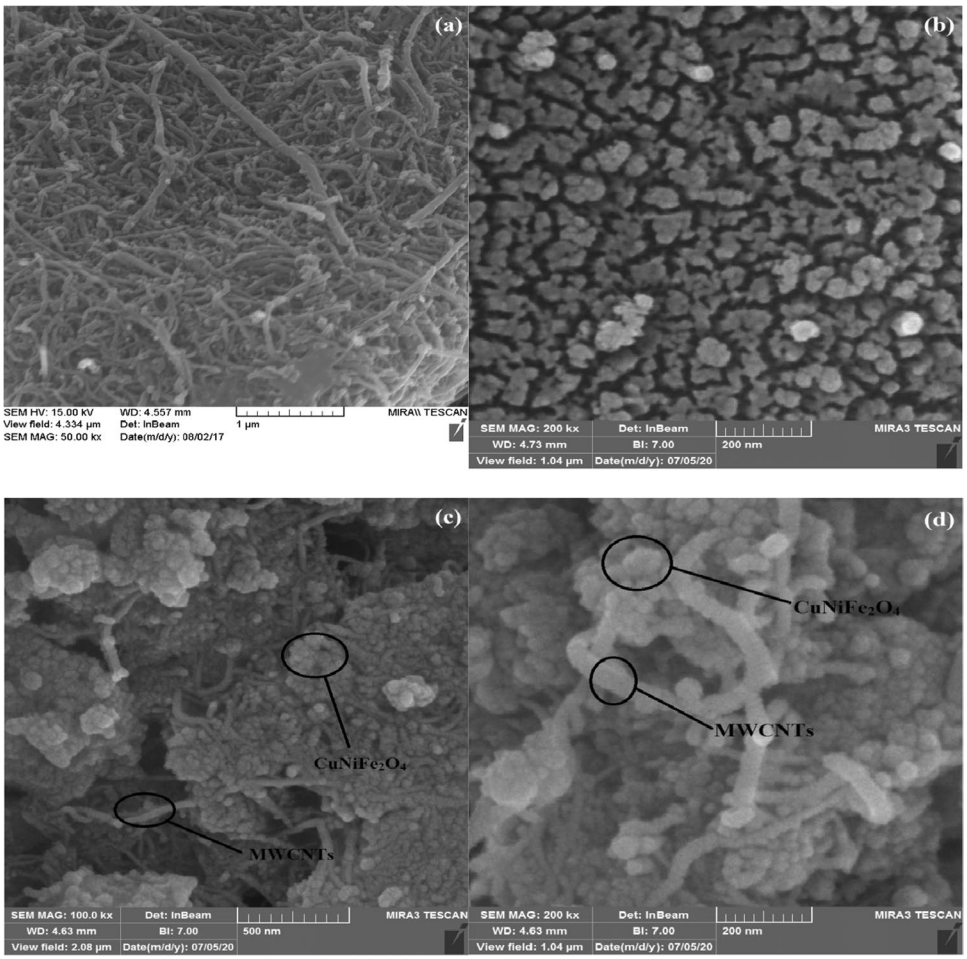

Fig. 2 SEM images of MWCNTs (**a**), $CuNiFe_2O_4$ (**b**), and MWCNTs-$CuNiFe_2O_4$ (**c** and **d**)

loaded with a high amount on supporting material. In addition, MWCNTs with numerous functional groups and high specific surface area can effectively increase the distribution of nanoparticles, as shown in Fig. 2a. To confirm the loading of ferrite nanoparticles on MWCNTs, TEM analysis was performed, and the results were shown in Fig. 3. It can be seen that the surface of MWCNTs was clean for nanoparticle loading (Fig. 3a), and $CuNiFe_2O_4$ nanoparticles were synthesized in a spherical shape by co-precipitation method (Fig. 3b). The nanoparticles are well loaded inside and outside the MWCNTs wall, indicating proper nanocatalyst synthesis for PMS activation and AMX degradation (Fig. 3c and d). Figure 4a shows that the ferrite particle distribution is very close and generally has a monodisperse structure. Identification of the catalyst structural composition was performed by EDX analysis, as shown in Fig. 4b. According to the present figure, the elements including Cu, Ni, and Fe were loaded on MWCNTs with weight percentages of 4.26, 3.06, and 24.71, respectively. The inset of Fig. 4b demonstrates the magnetic properties of the nanocatalyst and the loading of Fe on the supporting material. The elemental mapping results in Fig. 4c–g also confirmed the above results and showed a good distribution of the elements present on the MWCNTs in the electron micrograph region.

The FTIR spectra of MWCNTs and MWCNTs-$CuNiFe_2O_4$ were shown in Fig. 5a. In the FTIR spectrum of MWCNTs, peaks around 3419.29 cm^{-1} and 1400 cm^{-1} are related to O–H stretching. Peaks around 1030 cm^{-1}, 1647 cm^{-1}, and 2923 cm^{-1} are related to stretching vibrations of C-N, C = C, and C-H, respectively. After loading mixed ferrite on the MWCNTs, in addition to observing the peaks mentioned above, a broad band in the range of 550–650 cm^{-1} was observed which could be related to the metal ions coated on the substrate. The crystal structure of MWCNTs and MWCNTs-$CuNiFe_2O_4$ nanocatalyst is shown in Fig. 5b. The presence of diffraction peaks at $2\Theta = 24.7°$ and 42.5° is related to the graphite structure of CNTs. Analysis of XRD MWCNTs-$CuNiFe_2O_4$ in Fig. 5b shows seven distribution peaks at $2\theta = 16.96°$, 23.63°, 32.5°, 46.29°, 57.21°, 66.89°, and 76.05°. In this analysis, the sharp peak for CNTs has disappeared due to its destruction during the $CuNiFe_2O_4$ loading process. These XRD analysis results were similar to the synthesis reports of Khalifeh et al. [25] and Rajabzadeh et al. [38].

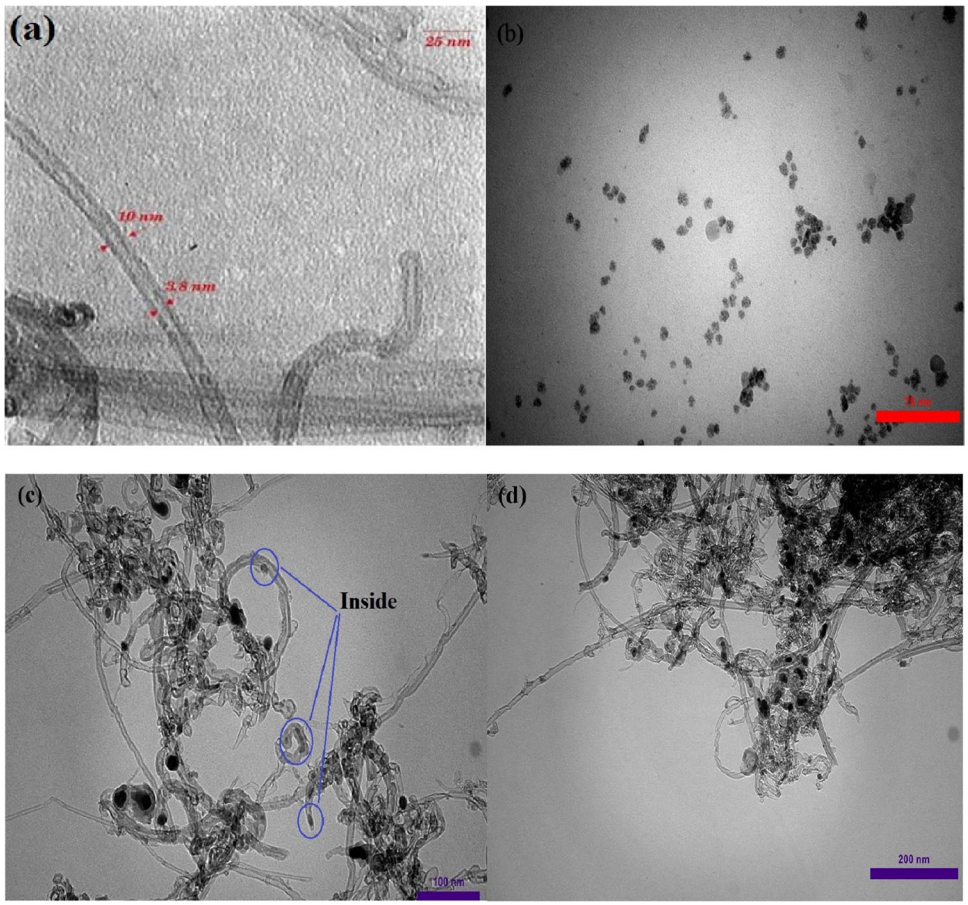

Fig. 3 TEM images of MWCNTs (**a**), $CuNiFe_2O_4$ (**b**), and MWCNTs-$CuNiFe_2O_4$ (**c** and **d**)

3.2 Effect of operational parameters

The initial pH is one of the important parameters in oxidation processes due to its effect on PMS decomposition and formation of different ionic charges on catalyst functional groups. Figure 6a shows the effect of initial pH on the degradation of AMX at PMS dosage of 2 mM, AMX concentration of 50 mg/L, and catalyst dosage of 250 mg/L. When the pH increases from 3 to 7, the AMX degradation efficiency improves from 73 to 100% at 120 min. However, with a further increase in pH above 8, the degradation efficiency decreased dramatically. The degradation efficiency changes in the studied pH range can be explained based on the zero charge point (PZC) of the catalyst and pKa of PMS. The zero charge point of MWCNTs-$CuNiFe_2O_4$ was measured at 7.85, which means that the surface charge of the catalyst becomes positive at pH < PZC, while the surface charge will be negative at pH > PZC. pKa_1 and pKa_2 of PMS were 0 and 9.4, respectively, which reveals that the HSO_5^- anion is the main species at pH less than 9.4, while the amount of SO_5^{2-} increases significantly at pH above 9.4. Guo et al. [39] reported that AMX has three different pKa values (2.4, 7.4, and 9.6) with acidic and alkaline functional groups. Therefore, AMX will mainly be present in the form of zwitterion at a certain pH range. Considering the ionization form of the material, when the pH is lower than 7.8, positive charge of MWCNTs-$CuNiFe_2O_4$ leads to increasing electrostatic adsorption of PMS and AMX, thus the production of ROSs to degrade AMX is enhanced at neutral pH. Similar results were reported by Dong et al. [40] for the degradation of bisphenol A by the kaolinite/$CuFe_2O_4$/PMS system. The decrease in the degradation efficiency of AMX at acidic pH may be related to the formation of H-bonds through the reaction of hydrogen ions (H^+) and the O–O bond of PMS. According to previous studies [40], the formation of a positive charge complex attached to HSO_5^- at an acidic pH limits the interaction of the dominant PMS species with the positive catalyst charge. In addition, high values of hydrogen ions reduce the decomposition rate through reaction with $SO_4^{\bullet-}$ and $HO^\bullet$ (Eqs. 1 and 2). Decrease process performance at alkaline pH may be related to the formation of depositable metal species and the negative surface charge of MWCNTs-$CuNiFe_2O_4$. Kermani et al. [41] reported that at high pH, $HO^\bullet$ radical is produced by the radical reaction of $SO_4^{\bullet-}$ with hydroxyl ion (OH^-). At the same time, $HO^\bullet$ is rapidly eliminated due to instability or becomes weaker reactive species by re-reacting with OH^- (Eq. 3).

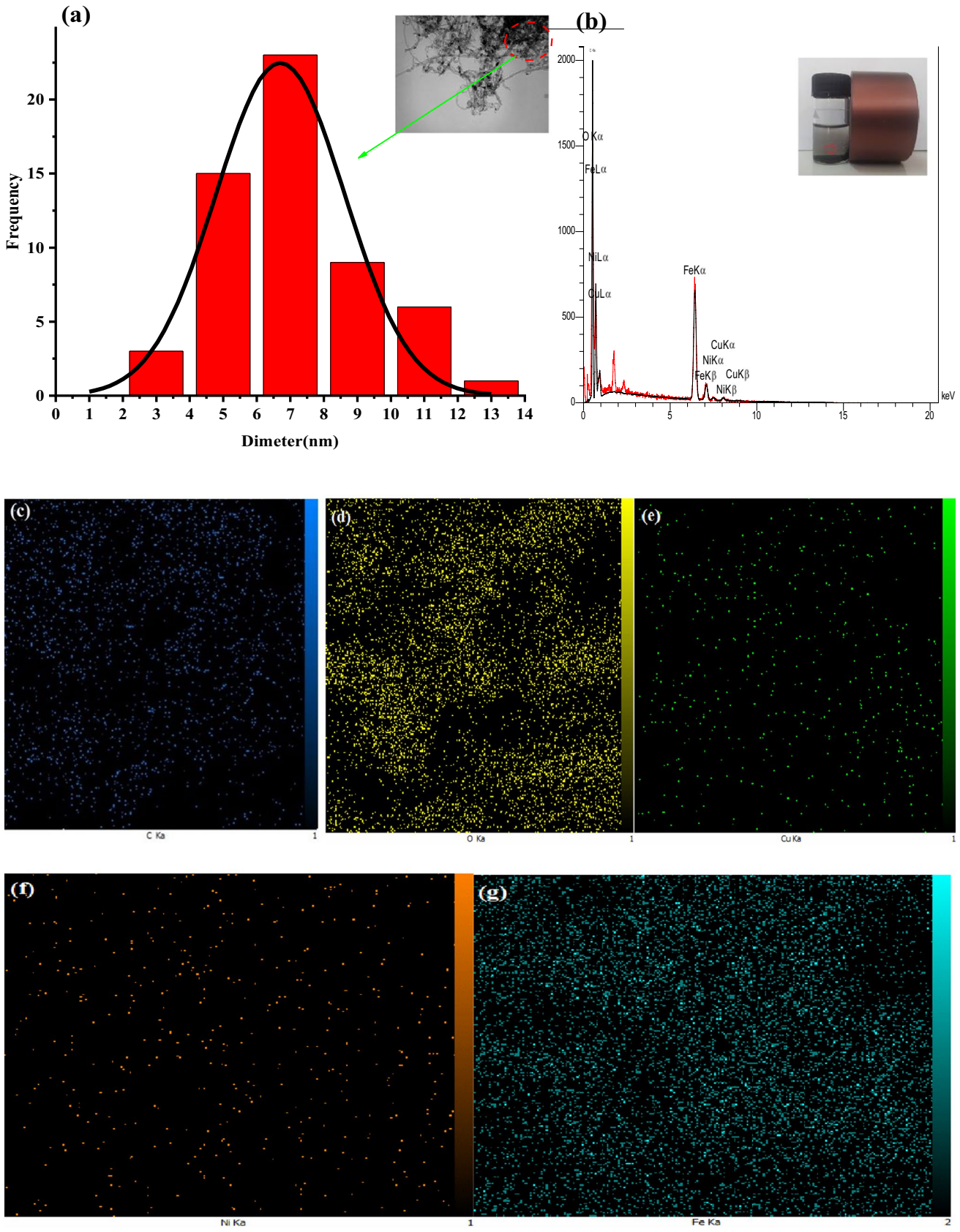

Fig. 4 Size histogram (**a**) and EDS spectrum (**b**) and EDS mapping (**c**–**g**) of MWCNTs $CuNiFe_2O_4$

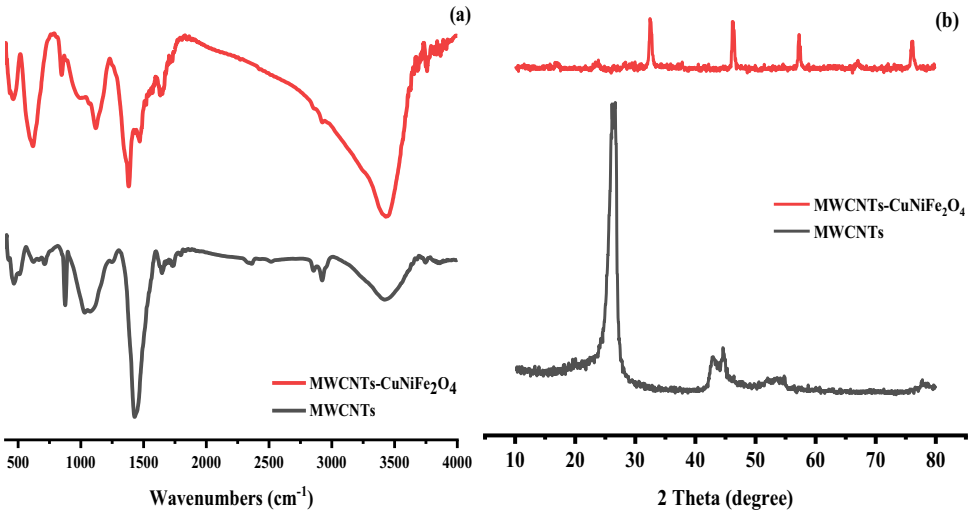

Fig. 5 FT-IR spectra (**a**) and XRD patterns (**b**) of MWCNTs and MWCNTs $CuNiFe_2O_4$

Figure 6b shows the effect of PMS dosage on AMX degradation efficiency at pH of 7, catalyst dosage of 250 mg/L, and AMX concentration of 50 mg/L. As expected, the degradation efficiency of AMX increased significantly from 64.08 to 99.52% when the PMS dosage increased from 0.5 to 5 mM at 80 min. This may be due to the production of more $SO_4^{\bullet-}$ and $HO^{\bullet}$ through high contact of HSO_5^- with the catalyst surface. Similar results were found by Qin et al. [42] for the degradation of biphenyls by the $CuFe_2O_4$/PMS system. With further increase of PMS from 5 to 7 mM, AMX degradation efficiency decreased from 99.52 to 90.23%. Therefore, 5 mM PMS was used as an oxidant dosage in subsequent experiments. High levels of PMS in reaction solutions can reduce the degradation efficiency of the contaminant through scavenge of active radicals and production of reactive species with lower redox potential ($E_0\ SO_5^{\bullet-} = 1.1$ V) (Eqs. 4 and 5). Peng et al. [43] reported similar results for the restricting effect of high PMS concentrations on the degradation efficiency of norfloxacin by Fe/Fe_3C@NG/PMS. Figure 6c shows the effect of MWCNTs-$CuNiFe_2O_4$ dosage on AMX degradation efficiency. When the catalyst dosage increased from 100 to 500 mg/L, the AMX degradation rate increased from 63.23 to 100% at 80 min. This enhancement may be due to an increase in the number of active sites for PMS adsorption and activation. When the amount of catalyst added to the reaction solution in the range of 750 to 1000 mg/L, the degradation efficiency is significantly reduced from 99 to 72.63%. This may be related to the rapid consumption of PMS to produce $SO_5^{\bullet-}$ and the scavenging effect of metal ions for radical species. In addition, the accumulation of high amount of particles on the catalyst may create a low surface area to adsorb contaminants and activate PMS. Liu et al. [44] found similar heterogeneous activation of PMS for the effect of $Bi_{25}FeO_{40}$ catalyst dosage. The results of the effect of the initial concentration of AMX on the degradation rate at pH of 7, catalyst dosage of 500 mg/L, and PMS dosage of 5 mM were shown in Fig. 6d. According to this figure, with increasing the concentration of AMX from 2 to 10 mg/L, the degradation rate in 60 min increased from 90.25 to 100%. This may be due to the greater access of AMX molecules to more ROSs during the catalytic process. Similar results were reported by Manu et al. [45] and Pourzamani et al. [46] for the removal of drugs by the AOPs. The results of Fig. 6d also show that 100 min of reaction time is required for complete degradation of 2 mg/L AMX. When the initial AMX concentration increases from 10 to 75 mg/L, the degradation rate decreases significantly from 100 to 72.36%. This reduction in efficiency at high concentrations of AMX can be explained as follows: When all operating parameters including pH, catalyst, and PMS dosage are constant, a certain amount of active radical is produced. This amount of radicals produced by the catalytic system can degrade a certain concentration of contaminants. Therefore, for high concentrations of pollutants, the amount of active radicals present in the environment will be inadequate. Similar results were reported for the degradation of organic pollutants by Fe_3O_4 [47] and G-$CoFe_2O_4$ [48] nanoparticles. The results of Fig. 6d generally emphasize that the MWCNTs-$CuNiFe_2O_4$/PMS reaction system has the ability to completely degrade AMX in the range of different concentrations at reaction times between 60 and 100 min.

$$^{\bullet}OH + H^+ + e^- \rightarrow H_2O \quad (1)$$

$$SO_4^{\bullet-} + H^+ + e^- \rightarrow HSO_4^- \quad (2)$$

$$^{\bullet}OH + OH^- \rightarrow H_2O + O^{\bullet-} \quad (3)$$

$$HSO_5^- + SO_4^{\bullet-} \rightarrow SO_4^{2-} + SO_5^{\bullet-} + H^+ \quad (4)$$

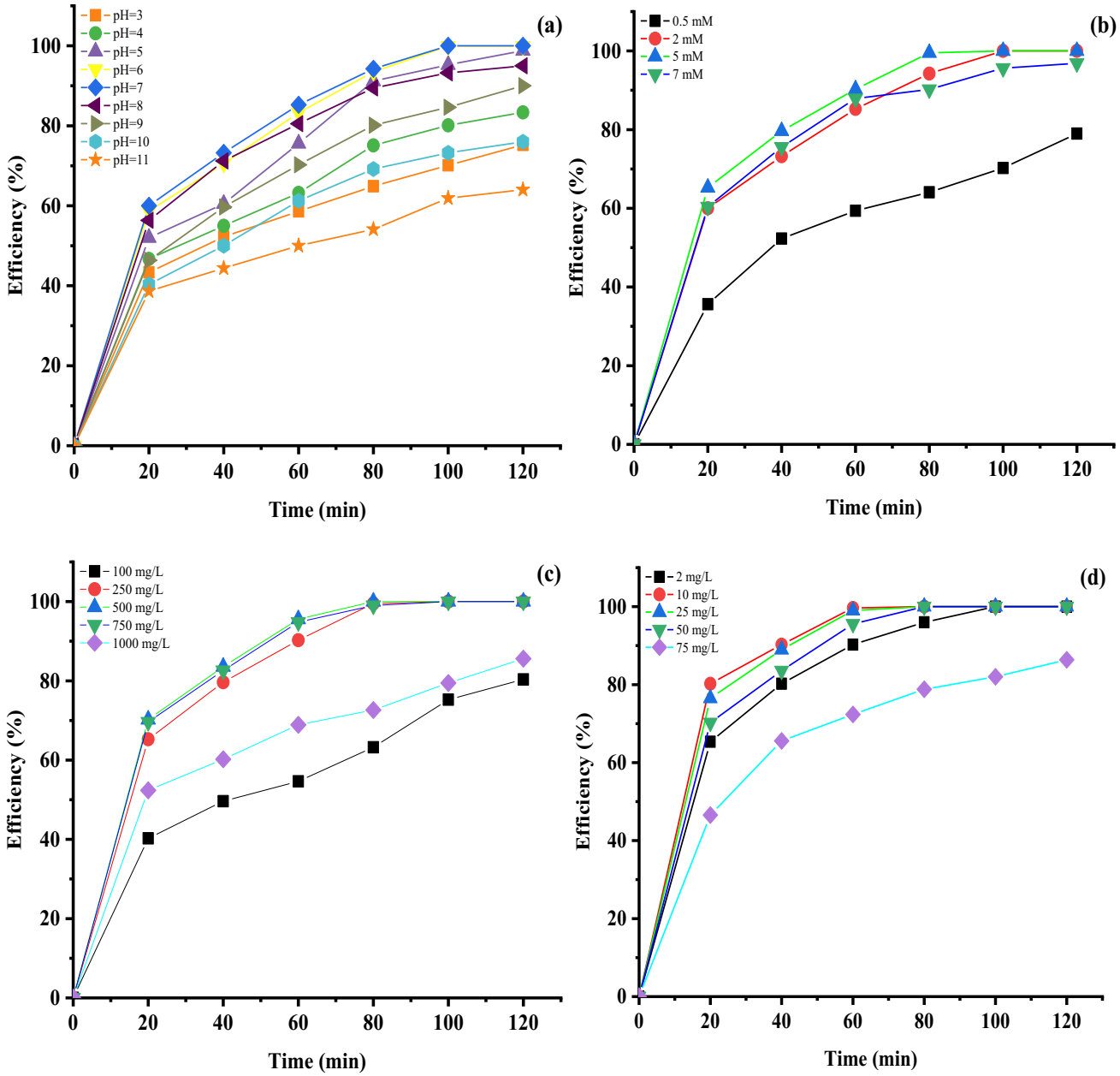

Fig. 6 Effect of the parameters on the degradation of AMX in the MWCNTs-$CuNiFe_2O_4$/PMS system. **a** Initial pH, **b** PMS dosage, **c** catalyst dosage, and **d** initial AMX concentration

$$HSO_5^- + {}^{\bullet}OH \rightarrow SO_5^{\bullet -} + H_2O \quad (5)$$

3.3 Catalytic activity of MWCNTs-$CuNiFe_2O_4$

To evaluate the catalytic activity of MWCNTs-$CuNiFe_2O_4$, comparative experiments were performed between different adsorption and oxidation systems at constant pH of 7, PMS dosage of 5 mM, catalyst dosage of 500 mg/L, and AMX concentration of 50 mg/L. As shown in Fig. 7a, MWCNTs-$CuNiFe_2O_4$ nanoparticles have an adsorption efficiency of 23.52% at 120 min. This low efficiency may be due to the reduction of active adsorption sites by filling the MWCNT pores with $CuNiFe_2O_4$ nanoparticles. The adsorption efficiency of MWCNTs (56.36%) was higher than that of MWCNTs-$CuNiFe_2O_4$. This may be due to freeness of CNT functional groups to adsorb pollutants. Similar results were reported by Mohammadi et al. [49] for the adsorption of AMX by MWCNTs.

The degradation rate of AMX in the reaction solution containing PMS was 28.9% at the reaction time of 120 min. Wang and Wang [50] reported that oxidants at different pH

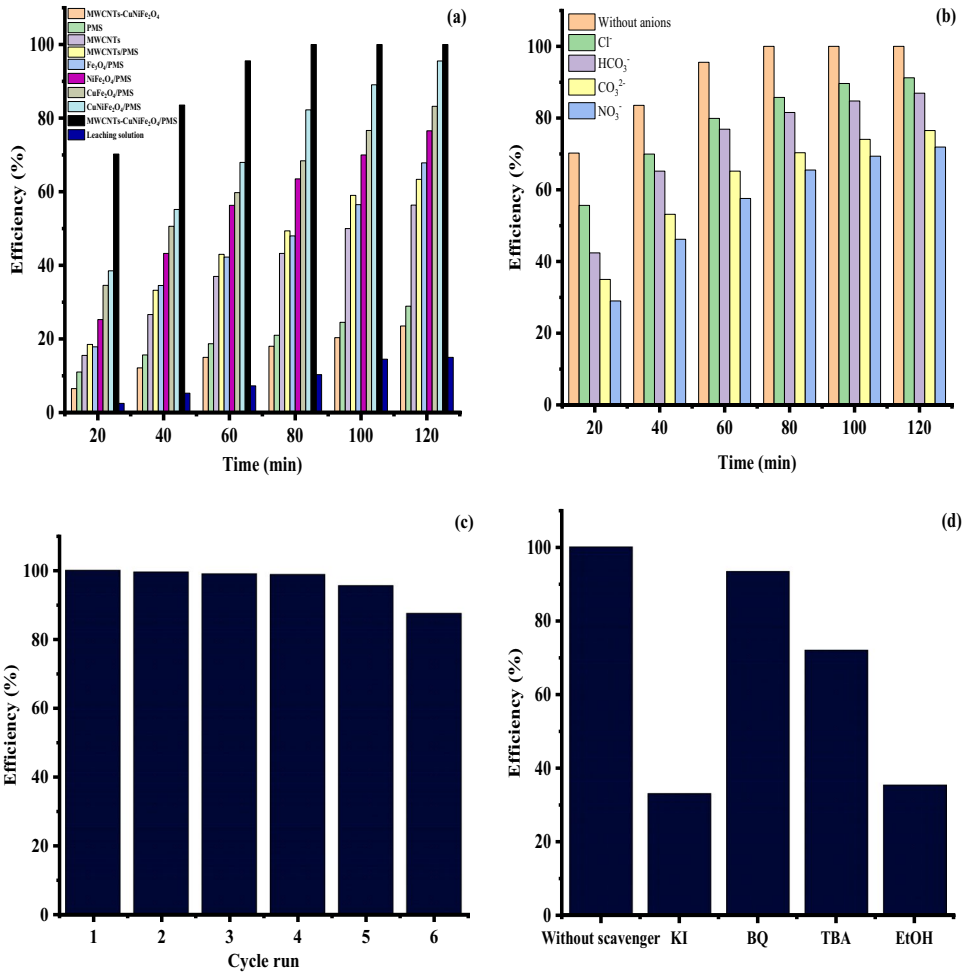

Fig. 7 AMX degradation in different processes (**a**), the effect of inorganic anions on AMX degradation (**b**), catalytic performance of MWCNTs-$CuNiFe_2O_4$ in continuous reaction cycle (**c**), and AMX degradation in the presence of radical scavengers in MWCNTs-$CuNiFe_2O_4$/PMS system (**d**)

values can be degraded into reactive species such as $HO_2^{\bullet}$, $O_2^{\bullet-}$, $SO_4^{\bullet-}$, and $HO^{\bullet}$ through nucleophilic attack. The amount and type of these reactive species vary from acidic to alkaline pH. When PMS is added to the solution containing MWCNTs, the removal rate of AMX is significantly increased compared to MWCNTs alone. This increase may be attributed to the transfer of electrons from the functional groups of MWCNTs to PMS to produce more reactive species. Similar results were reported by previous studies [35, 51, 52]. Similarly, by adding PMS to a solution containing Fe_3O_4, the degradation efficiency improves with increasing reaction time and the maximum efficiency of 67.85% occurs in 120 min. This increase in efficiency can be explained by the participation of the Fe(II)/Fe(III) cycle in the degradation of PMS into $SO_4^{\bullet-}$ and $HO^{\bullet}$. Compared to the above catalysts, $NiFe_2O_4$, $CuFe_2O_4$, and $CuNiFe_2O_4$ nanocomposites have the degradation efficiency of 76.56%, 83.2%, and 95.52%, respectively, at a reaction time of 120 min. This high efficiency of nanocomposites may be due to the interaction between metal ions to activate PMS for production of more active species. When the $CuNiFe_2O_4$ is loaded onto MWCNTs, complete degradation of AMX occurs in 80 min. This high efficiency may be related to the interaction between materials for AMX degradation and PMS activation. Moreover, the presence of MWCNTs in nanocomposites, in addition to producing reactive species through non-radical mechanisms, can facilitate the electron transfer between metal ions to reduce the catalytic center and electron transfer reaction in the oxidation of organic compounds. Hence, MWCNTs-$CuNiFe_2O_4$ could be a promising nanocatalyst for PMS activation to remove AMX.

3.4 Effect of common anions

It is well reported that anions such as chlorides are present in various industries wastewater due to their high consumption, and therefore, their presence in aqueous media has a negative effect on the degradation rate of organic pollutants. Figure 7b shows the effect of chloride ion (Cl^-) on the AMX degradation rate at pH of 7, catalyst dosage of 500 mg/L, and PMS dosage of 5 mM. According to this figure, the degradation efficiency of AMX in absence of anions was 100% at the reaction time of 80 min. However, with the addition of sodium chloride, the efficiency is dramatically

reduced to 85.76%. These efficiency changes may be related to the consumption of $SO_4^{\bullet-}$ and $HO^{\bullet}$ during the reaction and the formation of chloride-based active species (Eqs. 6–10). According to previous studies, these chloride species have lower oxidation potential (E_0 $Cl_2/2Cl^-$ = 1.36 V and E_0 $HOCl/Cl^-$ = 1.48 V) than $SO_4^{\bullet-}$. Similar results were reported by Yu et al. [53] for the oxidation of sulfamethoxazole by Co_3O_4-palygorskite/PMS.

$$HO^{\bullet} + Cl^- \leftrightarrow ClOH^{\bullet-} \tag{6}$$

$$SO_4^{\bullet-} + Cl^- \leftrightarrow SO_4^{2-} + Cl^{\bullet} \tag{7}$$

$$Cl^{\bullet} + Cl^{\bullet} \leftrightarrow Cl_2^{\bullet-} \tag{8}$$

$$Cl_2^{\bullet-} + Cl_2^{\bullet-} \rightarrow Cl_2 + 2Cl^- \tag{9}$$

$$Cl_2 + H_2O \rightarrow HOCl + H^+ + Cl \tag{10}$$

According to Henrys's law, carbon dioxide in the atmosphere is dissolved in the form of bicarbonate (HCO_3^-) in aqueous media and will therefore definitely be present in aqueous solutions. In the present study, the effect of HCO_3^- on the degradation efficiency of AMX has been investigated, and its results were shown in Fig. 7b. The degradation rate of AMX was reduced from 100 to 81.57% with the addition of HCO_3^-. This limitation in efficacy may be due to the production of active species of $CO_3^{\bullet-}$ with low redox potential through the reaction of HCO_3^- with $SO_4^{\bullet-}$ and $HO^{\bullet}$ (Eqs. 11 and 12). Similarly, the addition of CO_3^{2-} and NO_3^- can significantly reduce the degradation efficiency from 100 to 70.35% and 65.53%, respectively. According to previous studies [54], CO_3^{2-} would act as a scavenger for a large proportion of $SO_4^{\bullet-}$ and $HO^{\bullet}$ (Eqs. 13 and 14). Gao et al. [55] found similar results and reported that NO_3^- at the rate of 5.5×10^5 M^{-1} s^{-1} and $< 5.5 \times 105$ M^{-1} s^{-1} could consume $SO_4^{\bullet-}$ and $HO^{\bullet}$ to produce active nitrate (Eqs. 15 and 16).

$$HCO_3^- + SO_4^{\bullet-} \rightarrow HCO_3^{\bullet-} + SO_4^{2-} \tag{11}$$

$$HCO_3^- + HO^{\bullet} \rightarrow CO_3^{\bullet-} + H_2O \tag{12}$$

$$CO_3^{2-} + SO_4^{\bullet-} \rightarrow CO_3^{\bullet-} + SO_4^{2-} \tag{13}$$

$$CO_3^{2-} + HO^{\bullet} \rightarrow CO_3^{\bullet-} + OH^- \tag{14}$$

$$SO_4^{\bullet-} + NO_3^- \rightarrow SO_4^{2-} + NO_3^{\bullet} \tag{15}$$

$$^{\bullet}OH + NO_3^- \rightarrow NO_3^{\bullet} + OH^- \tag{16}$$

3.5 Catalyst stability and identification of reactive species

In terms of practical application and economic point of view, stability and reusability is one of the important parameters in oxidation systems. Therefore, the consecutive degradation reaction of AMX was performed in the presence of the recycled catalyst to activate PMS at pH 7, catalyst dosage of 500 mg/L, and PMS dosage of 5 mM. According to the results shown in Fig. 7c, the degradation rates of AMX remained the same during 4 consecutive reaction cycles. This may be due to the low loss of metallic species on MWCNTs during the catalytic reaction. However, by increasing the cycle from four to six, the efficiency decreased from 100 to 87.52%, which could be related to the loss of the recycled catalyst and the destruction of its surface during successive reactions. Nevertheless, the recycled catalyst has the potential to activate PMS for 4 cycles and can be used as a new and recyclable catalyst for AMX degradation. The more stability of MWCNTs-$CuNiFe_2O_4$ was evaluated by mixing 0.05 g of catalyst in 100 mL distilled water for 80 min to obtain a leaching solution. The results of ICP-MS demonstrated the leached Fe, Ni, and Cu concentration of 0.45 (4.5% of Fe used in the catalyst), 0.15 (3.8% of Ni used in the catalyst), and 0.22 mg/L (4.7% of Cu used in catalyst), respectively. The leaching solution was subsequently used to activate the PMS, and the results in Fig. 7b showed that the leaching solution could degrade less than 15% AMX. Hence, the synthesized catalyst has good stability for heterogeneous degradation of AMX.

To predict the mechanism of pollutant degradation by PMS activation, radical species need to be identified. Previous studies have reported that $SO_4^{\bullet-}$, $HO^{\bullet}$, $O_2^{\bullet-}$, and $SO_5^{\bullet-}$ radicals are produced during PMS activation, of which $SO_5^{\bullet-}$ is not normally responsible for the degradation of organic pollutants due to its low redox potential [56]. To identify active species in AMX catalytic decomposition, BQ, TBA, and EtOH were used for $O_2^{\bullet-}$, $HO^{\bullet}$, and both $SO_4^{\bullet-}$ and $HO^{\bullet}$ radicals, respectively. TBA without α-hydrogen reacts more with $HO^{\bullet}$ ($3.8–7.6 \times 10^8$ M^{-1} s^{-1}) compared to $SO_4^{\bullet-}$ ($4.0–9.1 \times 10^5$ M^{-1} s^{-1}), while EtOH containing α-hydrogen reacts easily with both radical species $SO_4^{\bullet-}$ ($1.6–7.7 \times 10^7$ M^{-1} s^{-1}) and $HO^{\bullet}$ ($1.2–2.8 \times 10^9$ M^{-1} s^{-1}) [57, 58]. As can be seen in Fig. 7d, in the presence of BQ, the AMX degradation was not significantly reduced compared to the control state (without scavenger). However, the degradation efficiencies decreased from 100 to 72.12% and 32.32% in the presence of TBA and EtOH, respectively. These results approved that both $SO_4^{\bullet-}$ and $HO^{\bullet}$ radicals participated effectively in the

degradation of AMX by the MWCNTs-$CuNiFe_2O_4$/PMS system.

Potassium iodide (KI) was used to scavenge adsorbed active species and to investigate PMS activation sites by catalyst. KI can effectively capture surface-bound radicals produced by nanocatalysts, while TBA or EtOH can trap all types of species produced in the system, such as free radicals and surface-bound radicals. As shown in Fig. 7d, by the addition of KI, the degradation of AMX is drastically reduced, which highlights that surface-bound radicals play an important role in the catalytic degradation of pollutants. Similar results were observed by Huang et al. [59] for the degradation of organic pollutants by the Co@ACFs/PMS system.

Based on the above results and previous studies [21, 35, 40], the mechanism of PMS decomposition by MWCNTs-$CuNiFe_2O_4$ has been proposed, and its schematic is shown in Fig. S8. As can be seen, a small amount of AMX can be adsorbed to catalyst-active sites, while another amount can be removed by spontaneous decomposition of PMS into active species. Degradation of PMS by MWCNTs also occurs through electron transfer from the catalyst surface to produce reactive species. In addition, PMS decomposition occurs in both the solution and solid phases. In the solution phase, the metals leached from catalyst decompose the PMS to produce $SO_4^{\bullet-}$ and $HO^{\bullet}$. In the solid phase (catalyst surface) the production of active species is done through the reaction of PMS molecules and transition metals such as Fe (II)/Fe (III), Cu (II)/Cu (III), and Ni (II)/Ni (III) in MWCNTs-$CuNiFe_2O_4$. In these reactions, metal species with an ionic charge of + 3 can be reduced by HSO_5^- to the forms Cu (II), Ni (II), and Fe (II). Finally, these reactive species produced can oxidize AMX to byproducts, CO_2 and H_2O.

3.6 Activation of various inorganic oxidants

The catalytic performance of MWCNTs-$CuNiFe_2O_4$ for AMX degradation was evaluated by activation of various oxidants (PMS, PS, and H_2O_2). Figure S9a shows the AMX degradation profile under the catalytic system at pH of 7, catalyst dosage of at 500 mg /L, PMS dosage of 5 mM, and AMX concentration of 50 mg/L. As can be seen, with increasing reaction time, the degradation efficiency of AMX in systems containing oxidants increases, which indicates the potential of MWCNTs-$CuNiFe_2O_4$ to activate PMS, PS, and H_2O_2. However, compared to the MWCNTs-$CuNiFe_2O_4$/PMS and MWCNTs-$CuNiFe_2O_4$/PS systems, a slight AMX removal was observed in the MWCNTs-$CuNiFe_2O_4$/H_2O_2 system, which may be due to restriction the H_2O_2 decomposition in neutral condition. In addition, the decrease in efficiency may be related to the non-selective performance and oxidation potential of $HO^{\bullet}$ produced by H_2O_2 decomposition, compared to the performance of $SO_4^{\bullet-}$ produced by PMS and PS decomposition. Similar results were observed for systems containing $Bi_{25}FeO_{40}$ [44] and iron anode [60] in the activation of different oxidants.

3.7 Mineralization and toxicity of AMX solution

The feasibility of the MWCNTs-$CuNiFe_2O_4$/PMS catalytic system has been investigated in terms of COD, TOC, and BOD_5 removal, and its results are shown in Fig. S9b. As can be seen, with increasing the reaction time from 20 to 120 min, the COD removal efficiency enhanced from 41.36 to 92%. Similarly, TOC removal efficiency improved from 24.45 to 69.69% when the reaction time increased from 20 to 120 min. This increase in mineralization may be related to the appropriate catalytic activity of MWCNTs-$CuNiFe_2O_4$ in the activation of PMS and the degradation of AMX over a long period of time. The results of Fig. S9b also showed that with increasing the reaction time from 20 to 120 min, the efficiency of BOD_5 removal increases from 23 to 64.58%. To evaluate the biodegradability of AMX solution, the BOD_5/COD rate was examined, and the results in inset of Fig. S9b showed that the BOD_5/COD rate increases from 0.14 to 0.49 with increasing reaction time. These results indicate that AMX can be converted to degradable compounds by the MWCNTs-$CuNiFe_2O_4$/PMS system.

In the present study, to evaluate the toxicity of the solution treated by MWCNTs-$CuNiFe_2O_4$/PMS, the optical density (OD) generated by *E. coli* and *S. aureus* was used. According to the toxicity analysis (Fig. S9c), the amount of OD for the untreated solution varied between 0–0.95 for *S. aureus* and 0–0.9 *for E. coli* at a reaction time of 1 to 24 h. When the AMX solution was treated, the OD value increases to 0–2 for *S. aureus* and 0–1.75 for *E. coli*. These results emphasize that the MWCNTs-$CuNiFe_2O_4$/PMS catalytic system can significantly reduce the toxicity of AMX solution.

3.8 AMX degradation pathways

Possible AMX degradation pathways were proposed based on the identification of intermediates by GC–MS. Seventeen products are found in the reaction system, and the results are presented in Fig. S10. In pathway I, by attacking the reactive species to the molecular structure of AMX, benzene and ([methylsulfonyl] methyl) (P1) can be formed. With further treatment, P1 may be converted to benzenesulfonic acid (P4) by substituting OH instead of CH_3 in the structure of byproducts. In the same pathway, P4 is oxidized to ethanone, 1-(4-methylphenyl (P10) by methylation. In the pathway I, P1 can also be oxidized to phthalic acid (P5) by deamination, disulfonation, and hydroxylation mechanisms, and then, by further treatment, is converted to benzoic acid, 2-nitro (P11). In pathway II, by breaking the carbon chains,

3-methylbenzothiophene (P2) is produced through the degradation of AMX and then, by increasing the reaction time, it can be oxidized to low molecular weight compounds such as 3,4-dimethylthiophene (P6) and 3-thiophenecarboxaldehyde (P7). In pathway 3, AMX is converted to H-benzimidazole-2-acetamide (P3) through bond cleavage by $SO_4^{\bullet-}$ and $HO^{\bullet}$. In the same pathway, P3 is oxidized to two products, i.e., m-nitroaniline (P8) and 1H-indole, 2-methyl (P9), by methylation. Byproduct P9 can be converted to 2-thiazolamine and 4,5-dihydro (P12) by dimethylation, sulfatination, and separation of the benzene ring. Finally, by opening the benzene rings, acids such as acetic acid, carbamic acid, propanoic acid, methoxyacetic acid, and sulfurous acid can be produced.

To further confirm the path of degradation and mineralization, measurements of NO_3^-, NH_4^+, and SO_4^{2-} concentrations in the treated solution were performed by ion chromatography. Figure S9d shows the values of NH_4^+, NO_3^-, and SO_4^{2-} in the operating conditions including pH of 7, MWCNTs-$CuNiFe_2O_4$ dosage of 500 mg/L, PMS dosage of 5 mM, and AMX concentration of 50 mg/L. As expected, with increasing reaction time from 1 to 24 h, the concentration of NH_4^+ formed increases from 3.56 to 6.8 mg/L. In the same solution, the NO_3^- concentration was below LOQ at 1 and 2 h and then slowly increased from 0.12 to 1.39 mg/L when the treatment time increased from 3 to 24 h. According to the structure of antibiotics, AMX has one sulfur atom and three nitrogen atoms. Catalytic decomposition of nitrogen to NH_4^+ and NO_3^- depends on the oxidation state of nitrogen. The results of Fig. S9d also show that the SO_4^{2-} anion is below LOQ in the first hour of the reaction, and it then increases from 0.05 to 8 mg/L, when the reaction time increases from 1 to 24 h. These results emphasize that the process of MWCNTs-$CuNiFe_2O_4$ can convert AMX to CO_2, H_2O, NH_4^+, NO_3^-, and SO_4^{2-} [61].

4 Conclusion

The MWCNTs-$CuNiFe_2O_4$ nanocatalyst was prepared as a new PMS activator by co-precipitation method and was used to degrade AMX. The characterize analysis proved that $CuNiFe_2O_4$ nanoparticles with good dispersion were loaded on the MWCNTs. MWCNTs-$CuNiFe_2O_4$ showed high catalytic activity in the degradation of AMX compared to homogeneous and heterogeneous catalysts, which may be related to the interaction between MWCNTs, Cu, Ni, and Fe to further activate PMS in the production of $SO_4^{\bullet-}$ and $HO^{\bullet}$. The degradation efficiency of AMX depends on the solution pH and is improved by increasing the pH from 3 to 7, however the alkaline pH (pH > 8) limits the AMX degradation rate. The AMX degradation rate increased with increasing catalyst and PMS dosages and decreased with increasing to values higher than the optimal range. The degradation rate decreased with the presence of different anions in the reaction medium due to their limiting effect on reactive species and the production of active radicals with low oxidation potential. In the MWCNTs-$CuNiFe_2O_4$/PMS system, the quenching test confirmed that both $SO_4^{\bullet-}$ and $HO^{\bullet}$ radicals could be involved in the effective degradation of AMX. MWCNTs-$CuNiFe_2O_4$ nanocatalysts showed stability and recyclability for 4 consecutive reaction cycles under optimal conditions including pH of 7, catalyst dosage of 500 mg/L, PMS dosage of 5 mM, and AMX concentration of 50 mg/L. Catalyst also showed high potential in activation of H_2O_2, PS and PMS. Suitable TOC removal efficiency and formation of NH_4^+, SO_4^{2-}, and NO_3^- in the MWCNTs-$CuNiFe_2O_4$/PMS process showed mineralization of pollutants and its products.. Toxicity study showed that the treated solution has a low limiting effect for *E. coli* and *S. aureus*. The AMX catalytic degradation pathways were proposed by GC–MS analysis. Based on the overall results, MWCNTs-$CuNiFe_2O_4$/PMS can be suggested as a promising system for the degradation of AMX from aqueous solutions due to catalyst stability, high mineralization efficiency, and reduced toxicity of the treated solution.

Supplementary Information The online version contains supplementary material available at https://doi.org/10.1007/s13399-022-02305-7.

Acknowledgements We are grateful for the financial support provided by the Department of Environmental Health Engineering of Larestan University of Medical Sciences (Grant No. 1397022).

Author contribution AR and NM: supervision, conceptualization, and funding acquisition. MD and MS: methodology and project administration. MM and MN: formal analysis and resources. HN and R: visualization and data curation. BN, MH, and SA: assistant experimenter and roles/writing—original draft. NM, MS, and MD: main writer and experimenter.

Data availability Supported by authors declaration.

Code availability Not applicable.

Declarations

Conflict of interest The authors declare no competing interests.

References

1. Sepehr MN, Allani F, Zarrabi M, Darvishmotevalli M, Vasseghian Y, Fadaei S, Fazli MM (2019) Data Brief 22:676–686
2. Dehghan A, Mohammadi AA, Yousefi M, Najafpoor AA, Shams M, Rezania S (2019) Nanomaterials 9:1422
3. Khosravi R, Zarei A, Heidari M, Ahmadfazeli A, Vosughi M, Fazlzadeh M (2018) Korean J Chem Eng 35:1000–1008
4. Dehghan A, Zarei A, Jaafari J, Shams M, Khaneghah AM (2019) Chemosphere 217:250–260

5. Hu J, Bian X, Xia Y, Weng M, Zhou W, Dai Q (2020) Sep Purif Technol 250:117109
6. Matsubara ME, Helwig K, Hunter C, Roberts J, Subtil EL, Coelho LHG (2020) Ecotoxicol Environ Saf 192:110258
7. Yousefi M, Gholami M, Oskoei V, Mohammadi AA, Baziar M, Esrafili A (2021) J Environ Chem Eng 9:105677
8. Taherkhani S, Darvishmotevalli M, Karimyan K, Bina B, Fallahi A, Karimi H (2018) Data Brief 19:1997–2007
9. Bian X, Xia Y, Zhan T, Wang L, Zhou W, Dai Q, Chen J (2019) Chemosphere 233:762–770
10. Verma M, Haritash A (2020) Environ Technol Innov 20:101072
11. Weng X, Cai W, Lin S, Chen Z (2017) Appl Clay Sci 147:137–142
12. Naghan DJ, Motevalli MD, Mirzaei N, Javid A, Ghaffari HR, Ahmadpour M, Moradi M, Sharafi K (2015) Bul Chem Commun 47:206–210
13. Mansourian N, Javedan G, Darvishmotevalli M, Sharafi K, Ghaffari H, Sharafi H, Arfaeinia H (2016) Int J Pharm Technol 8:13891–13907
14. Mohammadi H, Alinejad A, Khajeh M, Darvishmotevalli M, Moradnia M, Tehrani AM, Hosseindost G, Zare MR, Mengelizadeh N (2019) J Chem Technol Biotechnol 94:3158–3171
15. Ramírez-Franco JH, Galeano L-A, Vicente M-A (2019) J Environ Chem Eng 7:103274
16. Liu F, Cao J, Yang Z, Xiong W, Xu Z, Song P, Jia M, Sun S, Zhang Y, Zhong X (2021) J Colloid Interface Sci 581:195–204
17. Fadaei S, Noorisepehr M, Pourzamani H, Salari M, Moradnia M, Darvishmotevalli M, Mengelizadeh N (2021) J Environ Chem Eng 9:105414
18. Cui X, Liu X, Lin C, He M, Ouyang W (2020) Chemosphere 254:126820
19. Ghadari R, Namazi H, Aghazadeh M (2018) Appl Organomet Chem 32:e3965
20. Kazemi M, Ghobadi M, Mirzaie A (2018) Nanotechnol Rev 7:43–68
21. Kesavan G, Nataraj N, Chen S-M, Lin L-H (2020) New J Chem 44:7698–7707
22. Wang Z, Du Y, Liu Y, Zou B, Xiao J, Ma JJRA (2016) RSC Adv 6:11040–11048
23. Velinov N, Petrova T, Ivanova R, Tsoncheva T, Kovacheva D, Mitov I (2020) Hyperfine Interact 241:1–12
24. Kharisov BI, Dias HR, Kharissova OV (2019) Arab J Chem 12:1234–1246
25. Khalifeh R, Rajabzadeh M, Ebadi A (2019) Chemistry Select 4:13089–13093
26. Suharyadi E, Griyanika L, Utomo J, Agustina AK, Kato T, Iwata S (2018) Indones J Appl Phys 8:75–80
27. Afshin S, Rashtbari Y, Vosough M, Dargahi A, Fazlzadeh M, Behzad A, Yousefi M (2021) J Water Process Eng 42:102113
28. Yousefi M, Nabizadeh R, Alimohammadi M, Mohammadi AA, Mahvi AH (2019) Desalin Water Treat 158:290–300
29. Dehghani MH, Yetilmezsoy K, Salari M, Heidarinejad Z, Yousefi M, Sillanpää M (2020) J Mol Liq 299:112154
30. Mohammadi AA, Dehghani MH, Mesdaghinia A, Yaghmaian K, Es'haghi Z (2020) Int J Biol Macromol 155:1019–1029
31. Ghadiri SK, Alidadi H, Tavakkoli Nezhad N, Javid A, Roudbari A, Talebi SS, Mohammadi AA, Shams M, Rezania S (2020) Plos One 15:e0231045
32. Kouhpayeh A, Moazzen M, Jahed Khaniki GR, Dobaradaran S, Shariatifar N, Ahmadloo M, Azari A, Nazmara S, Kiani A, Salari M (2017) J Mazandaran Univ Med Sci 26:257–267
33. Eatemadi A, Daraee H, Karimkhanloo H, Kouhi M, Zarghami N, Akbarzadeh A, Abasi M, Hanifehpour Y, Joo SW (2014) Nanoscale Res Lett 9:393
34. Mujahid M, Khan RU, Mumtaz M, Soomro SA, Ullah S (2019) Ceram Int 45:8486–8493
35. Zhang X, Feng M, Qu R, Liu H, Wang L, Wang Z (2016) Chem Eng J 301:1–11
36. Singhal S, Sharma R, Singh C, Bansal S (2013) Indian J Mater Sci 2013: 1–7
37. Karthika V, Arumugam A (2016) Synthesis and characterization of MWCNT/TiO2/Au nanocomposite for photocatalytic and antimicrobial activity 11 113–118
38. Rajabzadeh M, Khalifeh R, Eshghi H, Bakavoli M (2018) J Catal 360:261–269
39. Guo W, Su S, Yi C, Ma Z (2013) Environ Prog Sustainable Energy 32:193–197
40. Dong X, Ren B, Sun Z, Li C, Zhang X, Kong M, Zheng S, Dionysiou DD (2019) Appl Catal B 253:206–217
41. Kermani M, Farzadkia M, Morovati M, Taghavi M, Fallahizadeh S, Khaksefidi R, Norzaee S (2020) J Environ Manag 266:110616
42. Qin W, Fang G, Wang Y, Zhou D (2018) Chem Eng J 348:526–534
43. Peng Q, Ding Y, Zhu L, Zhang G, Tang H (2018) Sep Purif Technol 202:307–317
44. Liu Y, Guo H, Zhang Y, Tang W, Cheng X, Li W (2018) Chem Eng J 343:128–137
45. Manu B, Mahamood R (2012) J Sustain Energy Environ 3:173–176
46. Pourzamani H, Mengelizadeh N, Hajizadeh Y, Mohammadi H (2018) Environ Sci Pollut Res 25:24746–24763
47. Tan C, Gao N, Deng Y, Deng J, Zhou S, Li J, Xin X (2014) J Hazard Mater 276:452–460
48. Pourzamani H, Jafari E, Rozveh M, Mohammadi H, Rostami M, Mengelizadeh N (2019) Desalin Water Treat 167:156–169
49. Mohammadi A, Kazemipour M, Ranjbar H, Walker RB, Ansari M (2015) Fuller Nanotub Carbon Nanostructures 23:165–169
50. Wang J, Wang S (2018) Chem Eng J 334:1502–1517
51. Lee H, Lee H-J, Jeong J, Lee J, Park N-B, Lee C (2015) Chem Eng J 266:28–33
52. Sun H, Kwan C, Suvorova A, Ang HM, Tadé MO, Wang S (2014) Appl Catal B 154:134–141
53. Yu Y, Ji Y, Lu J, Yin X, Zhou Q (2020) Chem Eng J 406:126759
54. Hassani A, Eghbali P, Kakavandi B, Lin K-YA, Ghanbari F (2020) Environ Technol Innov 20:101127
55. Gao Y, Zhao Q, Li Y, Li Y, Gou J, Cheng X (2021) Chem Eng J 405:126719
56. Rahmani A, Salari M, Tari K, Shabanloo A, Shabanloo N, Bajalan S (2020) J Environ Chem Eng 8:104468
57. Asgari G, Seid-Mohammadi A, Rahmani A, Samadi MT, Salari M, Alizadeh S, Nematollahi D (2021) Chemosphere 266:129179
58. Asgari G, Seid-mohammadi A, Rahmani A, Samadi MT, Alizadeh S, Nematollahi D, Salari M (2021) Sep Purif Technol 274: 118962
59. Huang Z, Bao H, Yao Y, Lu J, Lu W, Chen W (2016) J Chem Technol Biotechnol 91:1257–1265
60. Yang N, Cui J, Zhang L, Xiao W, Alshawabkeh AN, Mao X (2016) J Chem Technol Biotechnol 91:938–947
61. Motevalli M, Naghan D, Mirzaei N, Haghighi S, Hosseini Z, Sharafi H, Sharafi K (2015) Int J Pharm Technol 7:9672–9679